PNAS RESEARCH ARTICLE | CELL BIOLOGY

Ammonia transporter RhBG initiates downstream signaling and functional responses by activating NFκB

Saurabh Mishra[a,1], Nicole Welch[a,b,1], Shashi Shekhar Singh[a,1], Khuraijam Dhanachandra Singh[c], Annette Bellar[a], Avinash Kumar[a], Lars N. Deutz[a], Maxmillian D. Hanlon[a], Sashi Kant[a], Sumitava Dastidar[d], Hailee Patel[e], Vandana Agrawal[a], Amy H. Attaway[a,f], Ryan Musich[a], George R. Stark[g,2], Francesco Saverio Tedesco[d], George A. Truskey[e], I. David Weiner[h,i], Sadashiva S. Karnik[c], and Srinivasan Dasarathy[a,b,2]

Affiliations are included on p. 11.

Contributed by George R. Stark; received August 30, 2023; accepted June 19, 2024; reviewed by Christopher Adams and John McCarthy

Transceptors, solute transporters that facilitate intracellular entry of molecules and also initiate intracellular signaling events, have been primarily studied in lower-order species. Ammonia, a cytotoxic endogenous metabolite, is converted to urea in hepatocytes for urinary excretion in mammals. During hyperammonemia, when hepatic metabolism is impaired, nonureagenic ammonia disposal occurs primarily in skeletal muscle. Increased ammonia uptake in skeletal muscle is mediated by a membrane-bound, 12 transmembrane domain solute transporter, Rhesus blood group-associated B glycoprotein (RhBG). We show that in addition to its transport function, RhBG interacts with myeloid differentiation primary response-88 (MyD88) to initiate an intracellular signaling cascade that culminates in activation of NFκB. We also show that ammonia-induced MyD88 signaling is independent of the canonical toll-like receptor-initiated mechanism of MyD88-dependent NFκB activation. In silico, in vitro, and in situ experiments show that the conserved cytosolic J-domain of the RhBG protein interacts with the Toll-interleukin-1 receptor (TIR) domain of MyD88. In skeletal muscle from human patients, human-induced pluripotent stem cell-derived myotubes, and myobundles show an interaction of RhBG–MyD88 during hyperammonemia. Using complementary experimental and multiomics analyses in murine myotubes and mice with muscle-specific RhBG or MyD88 deletion, we show that the RhBG–MyD88 interaction is essential for the activation of NFkB but not ammonia transport. Our studies show a paradigm of substrate-dependent regulation of transceptor function with the potential for modulation of cellular responses in mammalian systems by decoupling transport and signaling functions of transceptors.

solute transporter | transceptor | hyperammonemia | skeletal muscle | NFkB

Significance

In plants and yeast, transceptors are membrane-bound solute transporters that also serve as sensors to initiate cellular signaling responses. In mammals, ammonia generated during physiological functions is converted to urea in hepatocytes for urinary excretion. Dysregulated ammonia metabolism with hyperammonemia occurs in a number of chronic diseases with increased transport into the skeletal muscle. We show that Rhesus blood group-associated B glycoprotein (RhBG), a mammalian ammonia transporter, interacts with myeloid differentiation primary response-88 (MyD88) and activates the transcription factor NFkB in mouse/human muscle. Unlike canonical activation of MyD88 via toll-like receptors, ammonia transport-dependent signaling is initiated by RhBG which functions as a transceptor. Decoupling transport-signaling functions of transceptors during cellular stress in mammalian systems has therapeutic potential beyond hyperammonemia.

Ammonia is an endogenous nitrogen metabolite that is generated during cellular amino acid and purine catabolism and by the gut microbiome (1). Hepatocyte ureagenesis is the major mechanism of ammonia disposal during physiological states with skeletal muscle uptake playing a minor role (2, 3). In a number of chronic diseases with impaired ammonia disposal (4), the systemic consequences include encephalopathy and cerebral edema (5). Skeletal muscle ammonia uptake during hyperammonemia (3, 6, 7) is believed to protect against more severe clinical consequences in patients with low muscle mass (8). The major mechanism of ammonia disposal in the skeletal muscle is by cataplerosis (loss of tricarboxylic acid cycle intermediates) of α-ketoglutarate (9), which results in mitochondrial dysfunction and reduced ATP synthesis (10, 11). Low cellular ATP content initiates adaptive responses to reduce cellular energy utilizing reactions (12). Since mRNA translation, a critical component of protein synthesis, requires high energy (13), a number of regulatory mechanisms are initiated to decrease cellular energy utilization (14). An adaptive mechanism to lower cellular energy demand is activation of NFκB (12), which inhibits skeletal muscle protein synthesis by transcriptional up-regulation of myostatin during hyperammonemia (7). Activation of NFκB during hyperammonemia results in transcriptional upregulation of myostatin, a transforming growth factor β superfamily member, that results in less protein synthesis and skeletal muscle loss (7, 15). However, the mechanism(s) by which ammonia activates NFκB is not currently known. Dissecting these mechanisms will potentially identify unique targets to protect the skeletal muscle while mitigating the systemic toxicity of ammonia.

During hyperammonemia, activation of inhibitor of κB (IκB) kinases (IKK) and nuclear translocation of NFκB have been reported (7), but the mechanism by which this pathway is activated is not known. Canonical activation by phosphorylation and nuclear translocation of NFκB occurs rapidly upon exposure to proinflammatory extracellular molecules

Reviewers: C.A., Mayo Clinic; and J.J.M., University of Kentucky.

The authors declare no competing interest.

[1]S.M., N.W., and S.S.S. contributed equally to this work.

[2]To whom correspondence may be addressed. Email: dasaras@ccf.org or starkg@ccf.org.

This article contains supporting information online at https://www.pnas.org/lookup/suppl/doi:10.1073/pnas.2314760121/-/DCSupplemental.

Published July 25, 2024.

including pathogens and cytokines via toll like receptor (TLR) mediated downstream signaling pathways (16, 17). Of the various reported TLRs, expression and responses to TLR4 stimulation are most robust in skeletal muscle and myotubes (18, 19). We therefore evaluated whether the canonical TLR4-dependent mechanism is responsible for activation of NFκB during hyperammonemia. The signaling cascade downstream of TLRs includes myeloid differentiation primary response-88 (MyD88), a signaling adaptor for the inflammation pathway that results in phosphorylation and nuclear translocation of NFκB (20, 21). Activation of NFκB during hyperammonemia has been reported in multiple organs/cellular systems, including skeletal muscle and myotubes (7, 22). Whether the signaling pathway upstream of NFκB during hyperammonemia is MyD88-dependent is not known. Downstream signaling from MyD88 involves interaction of the Toll-interleukin-1 receptor (TIR) domain with other TIR domain-containing receptors/activators, including TLRs (23). The N-terminal death domain (DD) on MyD88 associates with the interleukin-1 receptor associated kinase (IRAK) family members (24, 25). The Myddosome complex forms a scaffold for the Lysine (K) 63 polyubiquitination of tumor necrosis factor receptor associated factor-6 (TRAF6) kinase activation with phosphorylation of transforming growth factor-β-activated kinase-1 (TAK1). The consequent phosphorylation and activation of IKK results in phosphorylation and nuclear translocation of NFκB (23). Large molecules, including lipid A, are reported ligands for the activation of the TLR-MyD88 inflammatory cascade (26), but whether this pathway is activated by a small molecule like ammonia is not known. Identifying the mechanism of activation of the NFκB–myostatin axis during hyperammonemia has translational relevance because the functional consequences contribute to dysregulated proteostasis (4, 15).

A number of ammonia transporters have been described in different organisms (27–29). The Rh glycoprotein family of ammonia transport proteins are selectively expressed in tissues involved in ammonia metabolism in humans and non-human mammals (28, 30, 31), but it is not known whether these proteins have functions other than transport. Recently, membrane proteins that are regulated by the presence or absence of extracellular substrates and have both solute transport and receptor-like signaling activities have been termed transceptors (27, 32–34). Transceptors described to date, including those in nonmammalian systems like yeast and plants (32, 35), have substrate-induced trafficking controls with increased expression during substrate-depleted states and a rapid decrease in expression upon substrate availability (36, 37). In yeast, the ammonia transporter Mep2, but not Mep1 or Mep3, functions as a transceptor (38). In mammalian tissues, it is not known whether Mep2 ortholog(s) function as mediators of ammonia-dependent downstream signaling responses. Transporters for ammonia in mammals include the regulated Rhesus blood group-associated B glycoprotein (RhBG) protein (31), a putative polytopic 12 transmembrane protein based on homology modeling from the related Rhesus blood group–associated glycoprotein (RhCG) ammonia transporter (39). RhCG is a constitutively expressed ammonia transporter in skeletal muscle (31), but it is not known whether RhCG functions as a transceptor. However, RhBG is transcriptionally up-regulated in skeletal muscle in the presence of high extracellular ammonia concentrations (31).

In the present studies, we show that the RhBG transmembrane protein serves as an ammonia transporter, and its conserved C-terminal region interacts with the cytosolic adapter protein, MyD88, to initiate the canonical activation of NFκB with subsequent transcriptional upregulation of myostatin. We also show that the interaction between RhBG and the TIR domain of MyD88 is required for signaling but not for ammonia transport. Complementary bioinformatics analyses of transcriptomics also showed that NFκB-dependent signaling is regulated by RhBG and MyD88. Thus, RhBG functions is a bifunctional molecule with ammonia transport and MyD88-dependent signaling functions during hyperammonemia in mammalian cells. These data provide the basis for developing decoupled interventions that maintain ammonia transport but inhibit adverse signaling responses thereby preventing cytotoxicity and tissue injury during hyperammonemia.

Results

Hyperammonemia Activates NFκB with Increased Expression of Myostatin Via the Canonical MyD88 Pathway. Hyperammonemia resulted in the phosphorylation and activation of NFκB and its transcriptional target, myostatin, with impaired mTORC1 signaling in skeletal muscle from patients with cirrhosis, human-induced pluripotent stem cell (hiPSC)-derived myotubes, and myobundles on bioengineered matrices (Fig. 1 *A*–*E*). These molecular responses are similar to those reported in hyperammonemic murine myotubes and rodent models (7, 40). Canonical activation of NFκB occurs via the MyD88–IRAK-dependent activation of the downstream kinase, TAK1 (23, 24). During hyperammonemia, phosphorylation of IRAK4 is increased, suggesting a MyD88-dependent activation of NFκB (Fig. 1*A*).

During hyperammonemia, MyD88-dependent increased phosphorylation of p65-NFκB was noted in murine myotubes (Fig. 2*A*). In immunoprecipitation and immunoblot studies, the canonical pathway of activation of NFκB is initiated by binding of MyD88 to IRAK4 (Fig. 2*B*). The downstream pathway activation that includes binding of TRAF6 to IRAK4 and consequent K63 ubiquitination of TRAF6 was observed (Fig. 2 *C* and *D*). The K63 ubiquitinating modification of TRAF6 allows for scaffolding function and activation of downstream TAK1 (41). We noted TRAF6 was bound to TAK1 during hyperammonemia (Fig. 2*E*). Phosphorylation of TAK1 during hyperammonemia was identified by electrophoresis mobility shift as well as increased phosphorylation of serine and threonine in TAK1 immunoprecipitates in murine myotubes and skeletal muscle from the portacaval anastomosis rat (Fig. 2 *F* and *G*). These data show that canonical MyD88–mediated activation of NFκB is intact during hyperammonemia in skeletal muscle.

Canonical activation of MyD88 occurs via recruitment to ligand bound pathogen recognition TLRs, of which TLR4 is one of the most highly expressed (*SI Appendix*, Fig. S1) with robust signaling responses in skeletal muscle (18, 19). Expression of TLR (2, 4, 6) mRNA in murine myotubes did not change during hyperammonemia at 6 and 24 h of ammonia treatment (Fig. 3*A*). Genetic depletion of TLR4 in murine myotubes inhibited both activation (nuclear translocation) of NFκB and degradation of IKBα with lipopolysaccharide but not with hyperammonemia (Fig. 3*B*). These data show that activation of NFκB is TLR4-independent during hyperammonemia while canonical responses to lipopolysaccharide were maintained. Activation of p65-NFKB occurred with MyD88 knockout alone and did not change with hyperammonemia (Fig. 3*C*). Consistent with activation of NFκB, expression of IKBα was lower with hyperammonemia in wild type (WT) but not in myotubes with MyD88 knockout (Fig. 3*D*). Hyperammonemia increased activation of p65-NFκB and expression of its downstream target, myostatin, in WT but not in MyD88 knockout myotubes (Fig. 3*E*). These data show that hyperammonemia induces activation of NFκB and increased expression of myostatin, a transcriptional target of NFκB (7). These responses occur by sequential activation/binding of molecules in the canonical MyD88 pathway by a TLR4-independent mechanism.

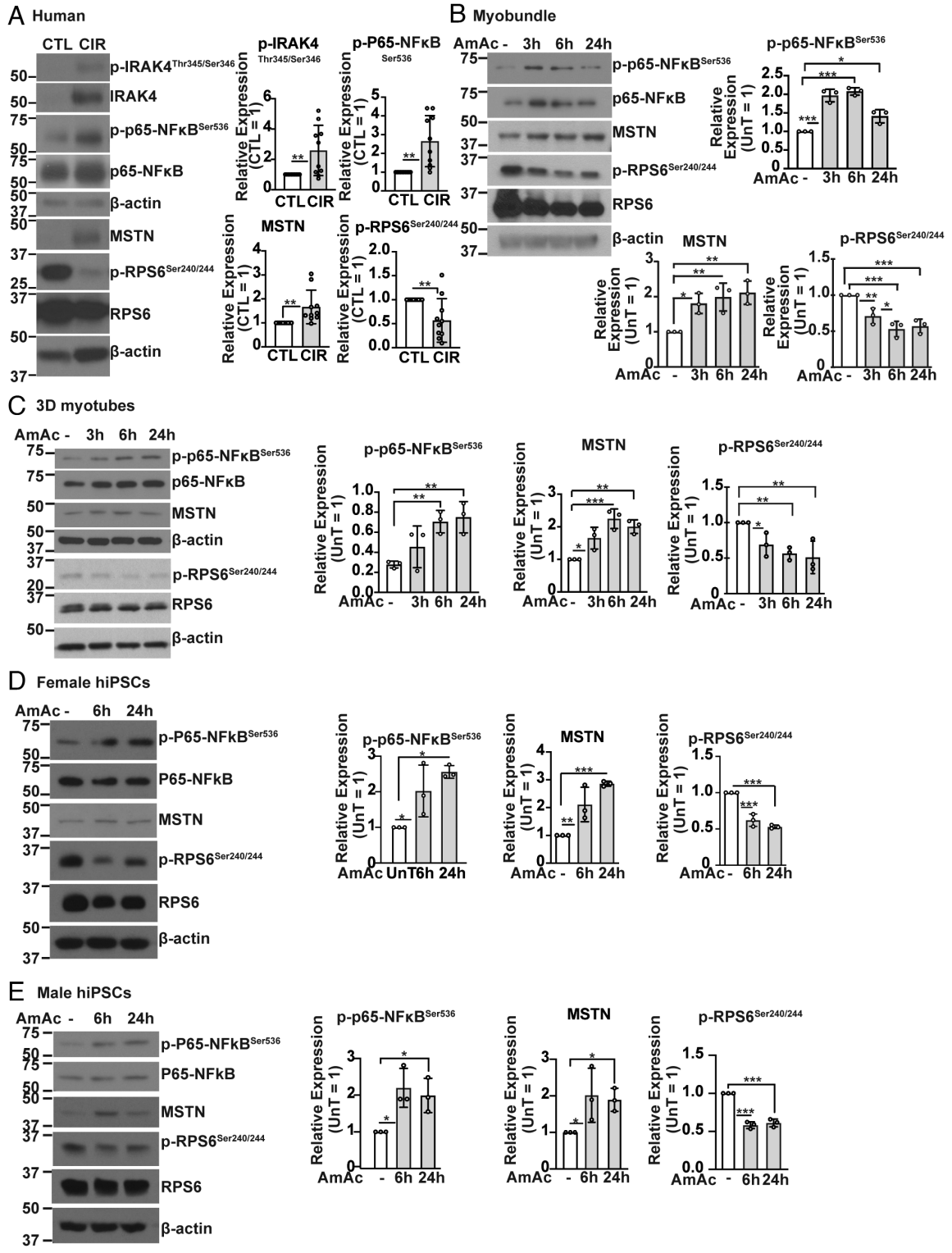

Fig. 1. Activation of NFκB–myostatin axis in a comprehensive array of hyperammonemic skeletal muscle models. Representative immunoblots and densitometries from specified models with/without hyperammonemia. (*A*) p-IRAK4, p-p65-NFκB, myostatin, and p-RPS6 in skeletal muscle of healthy and cirrhosis patients. (*B*) p-p65-NFκB, myostatin, and p-RPS6 in engineered or biomimetic human skeletal muscle culture system ("myobundle"). (*C*) p-p65NFκB, myostatin, and p-RPS6 in 3D artificial skeletal muscle constructs derived from human immortalized myoblasts. (*D* and *E*) p-p65-NFκB, myostatin, and p-RPS6 in human iPSC-derived skeletal myotubes (female, male) at stated times of treatment with 10 mM ammonium acetate. All data mean ± SD from 10 biological replicates in human skeletal muscle and three biological replicates in myobundles and myotubes. **P* < 0.05, ***P* < 0.01, ****P* < 0.001. Student's *t* test was used for all 2-group comparisons; ANOVA with uncorrected Fisher LSD multiple comparison test was used for all multiple-group comparisons. Representative loading controls (β-actin) are shown for p-NFkB/NFkB and myostatin in panel *A*; and p-RPS6/RPS6 for panel *B*; p-P65-NFkB and RPS6 for panel *C*; p-RPS6/myostatin for panel *D*; myostatin for panel *E*; and all lanes shown for each protein are from the same biological replicate.

Regulated Ammonia Transporter Protein, RhBG, Interacts with MyD88 During Hyperammonemia. We then evaluated the mechanism by which the regulated ammonia transporter RhBG initiates the MyD88 signal transduction responses. Immunoprecipitation studies showed increased association of MyD88 with ammonia transporter, RhBG (Fig. 4*A*) and IRAK4, a mediator of downstream signaling

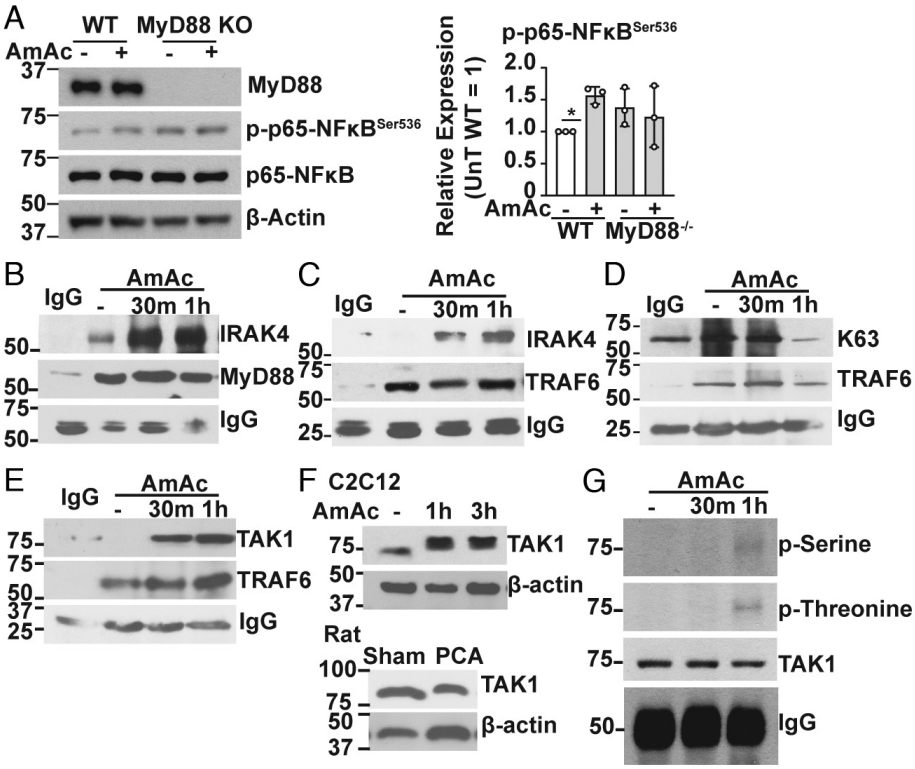

Fig. 2. Intact MyD88–TAK1 (Myddosome) axis during hyperammonemia activates NFκB. Studies done in C2C12 murine myotubes treated without/with hyperammonemia or gastrocnemius muscle from hyperammonemic portocaval anastomosis (PCA) or sham-operated control male Sprague Dawley rats. (*A*) Representative immunoblots and densitometry of p-p65-NFκB with deletion of MyD88 in myotubes. (*B*) Representative immunoblots of IRAK4 in immunoprecipitates of MyD88 in myotubes. (*C*) Immunoprecipitate of TRAF6 probed for IRAK4 in myotubes. (*D*) Ubiquitination of lysine63 in immunoprecipitates of TRAF6 in myotubes. (*E*) Representative immunoblots of TRAF6 immunoprecipitates probed for TAK1 in myotubes. (*F*) Representative immunoblots of TAK1 gel shift in myotubes and gastrocnemius muscle. (*G*) Representative immunoblots of serine and threonine phosphorylation of TAK1 in myotubes. All data for the immunoblots that show mean ± SD (panel *A*) and gel shift experiments (panel *F*) are from at least 3 biological replicates. **P* < 0.05. Immunoprecipitation experiments were done in n = 1. ANOVA with Fisher uncorrected LSD post hoc analysis was used for multiple group comparisons. For panels containing multiple immunoblots, representative blots shown are from the same biological replicate. Representative loading controls (β-actin) originate from the following blots: panel *A*. p-P65NFκB; panel *G*: p-Threonine. Myotubes were treated with 10 mM ammonium acetate for the stated times.

responses during hyperammonemia in murine myotubes (Fig. 4*B*). Blocking ammonia transport with methylammonium (Fig. 4*B* and *SI Appendix*, Fig. S2) prevents the MyD88–IRAK4 association. These data suggest that during hyperammonemia, MyD88 binds to RhBG and initiates downstream signaling responses with phosphorylation and activation of NFκB that is independent of TLR4.

RhBG is a 12-transmembrane protein of which the C-terminal contains a conserved 7/J-domain (42, 43). The TIR domain of MyD88 is responsible for interaction with TLRs, including TLR4, and a DD initiates downstream signaling responses (20, 21). To test the hypothesis of an RhBG–MyD88 interaction, we performed in silico, in vitro, and in situ experiments. Initially, in silico docking studies were performed between the conserved 7/J-domain of RhBG and the death and TIR-domains of MyD88 to determine the mechanism of RhBG–MyD88 interaction (*SI Appendix*, Fig. S3 *A*–*C*). We observed that the Arg413, Asp418, Pro420, and Asp428 residues in the conserved 7/J-domain of RhBG can interact with the Gln173, Glu177, Lys282, Trp284, Arg288, and Lys291 residues of MyD88 on the TIR domain (Fig. 4*D*). Validation studies using GST-tagged proteins for each of the cytosolic domains of RhBG incubated with lysates from differentiated murine myotubes and then probed for MyD88 showed that the strongest interaction was between the 7/J-domain of RhBG and the TIR domain of MyD88 (Fig. 4*E*). Studies using surface plasma resonance (SPR) showed an interaction between MyD88 and RhBG with a full-length C-terminal but not the RhBG construct with deletion of the 7/J-domain on the C-terminal. Nonspecific interaction with GST and MyD88 did not occur (Fig. 4*F*). These results confirm our hypothesis that the 7/J-domain of RhBG interacts with the TIR-domain of MyD88.

Complementary studies using fixed and live-cell imaging performed in WT murine C2C12 myotubes transfected with eGFP-tagged full-length RhBG and mCherry-tagged full-length MyD88 also showed greater interaction during hyperammonemia (Fig. 4 *G* and *H* and *SI Appendix*, Fig. S3*D* and Video S1). These complementary data show that the cytosolic, C-terminal 7/J-domain on the ammonia transporter, RhBG, interacts with MyD88 during hyperammonemia.

Specific Sites on TIR Domain on MyD88 Mediate Signaling Responses During Hyperammonemia. Having established that an interaction between RhBG and MyD88 was required for signaling responses but not ammonia transport, we then determined the specific sites on MyD88 that mediate the signaling responses during hyperammonemia. We experimentally validated the interaction between RhBG and specific sites on MyD88 (identified in silico) and subsequent downstream functional responses by expressing full-length and mutant MyD88 TIR domains in MyD88 knockout murine myotubes. Hyperammonemia-induced increase in phosphorylation of p65-NFκB was not observed in MyD88 knockout myotubes (even though there is increased phosphorylation of p65-NFκB in untreated myotubes with MyD88 knockout) (Fig. 5*A*). Thus, when the interactions between MyD88–RhBG are disrupted through site-directed mutagenesis in MyD88, downstream signaling and activation of NFκB were not observed. Based on our molecular docking

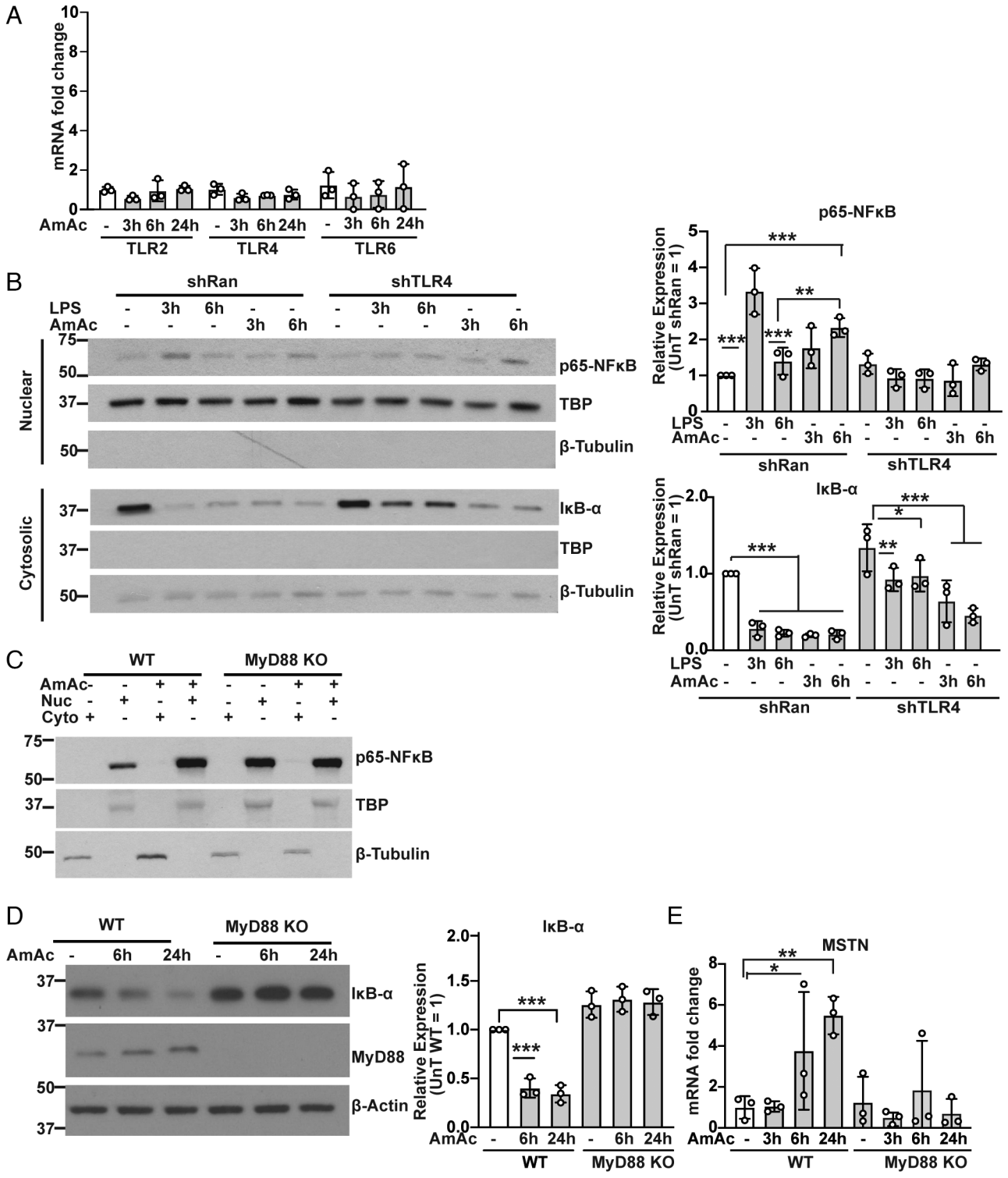

Fig. 3. Non-canonical activation of MyD88 during hyperammonemia. All studies done in untreated or 10 mM ammonium acetate (AmAc) treated (for the specified timepoints) hyperammonemic, differentiated, murine C2C12 myotubes. (*A*) Relative mRNA levels of TLR2, TLR4, and TLR6. in C2C12 myotubes. Representative immunoblots and densitometry (*B*–*E*). (*B*) p65-NFκB and IκB-α in nuclear and cytosolic fractions in TLR4 depleted myotubes. (*C*) p65-NFκB in the nuclear and cytosolic fraction in myotubes with or without MyD88 KO (knockout). TBP and β-tubulin are markers for nucleus and cytosol fractions respectively. (*D*). IκB-α in WT or MyD88 KO. (*E*) Relative mRNA expression of myostatin gene in WT and MyD88 KO. TATA binding protein (TBP) and β-tubulin were used to show the cellular fraction (nucleus/cytosol). All data for the immunoblots that show mean ± SD are from at least three biological replicates. **P* < 0.05, ***P* < 0.01, ****P* < 0.001. ANOVA with Fisher uncorrected LSD post hoc analysis was used for multiple group comparisons. For panel *D*, lanes shown are from the same biological replicates. Representative loading control (β-actin) for panel *D* originates from the IκB-α blot.

studies (Fig. 4*D*), we generated single (Lys282Ala, Trp284Ala, Trp286Ala, and Arg288Ala) and double (Trp284Ala + Arg288Ala and Trp286Ala + Arg288Ala) mutants of MyD88. Since in silico studies suggested that Gln173, Gln177, and Lys291 on the TIR domain of MyD88 interact with the terminal residues of the RhBG 7/J-domain peptide (C- and N-terminal of the peptide), these sites were excluded from the mutagenesis experiment. Our data suggest that overexpression of the TIR domain in WT myotubes potentially competes with the FL-MyD88, due to its small size, and occupies the RhBG binding site. As a result, FL-MyD88 is

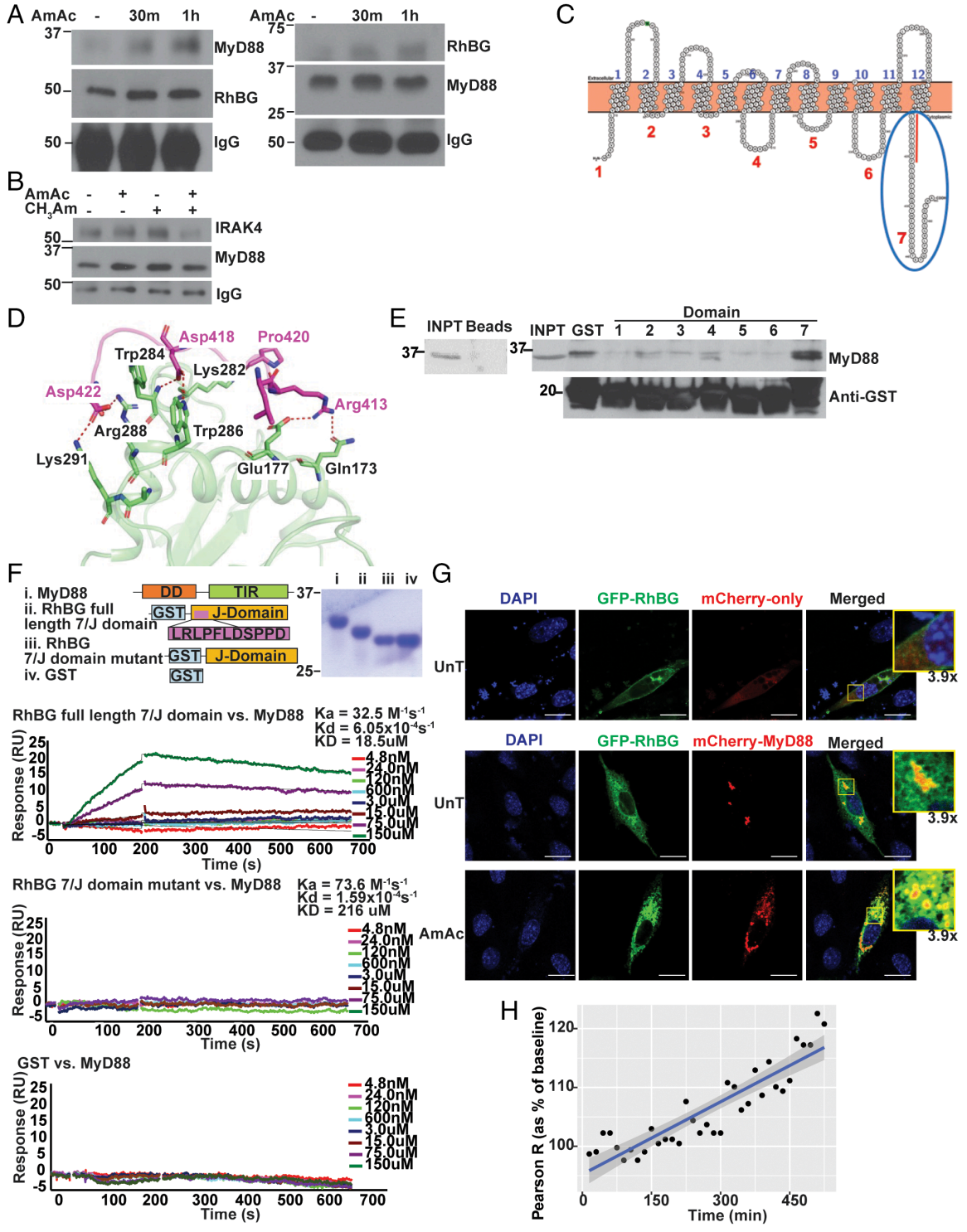

Fig. 4. Molecular docking with experimental validation showed potential interactions between the conserved C-terminal peptide of RhBG and TIR domain on MyD88. (*A*) Representative immunoblots of MyD88 in immunoprecipitates of RhBG and immunoblots of RhBG in immunoprecipitates of MyD88 from myotubes during hyperammonemia. (*B*) Representative immunoblots of IRAK4 in immunoprecipitates of MyD88 in myotubes during hyperammonemia or untreated controls with/without methylammonium to block intracellular ammonia entry. (*C*) Snake plot of RhBG protein displaying transmembrane, extracellular, and intracellular regions with the C-terminal J-domain (blue oval) with the conserved region (vertical line adjacent to the descending limb). (*D*) Conserved C-terminal with LPFLDSPPR domain interacts with known conserved C-terminal of TIR domain of MyD88. (*E*) In vitro interaction of MyD88 with RhBG cytoplasmic domain. GST-RhBG cytoplasmic domains were purified with a glutathione–Sepharose column were bound to glutathione–Sepharose beads, Equal amount of C2C12 myotubes crude lysate was added and pulled down was done with Glutathione–Sepharose beads followed by western with MyD88 antibody. (*F*) Schematic diagram of MyD88 and different construct of RhBG7 (left upper) and Coomassie blot of purified proteins (left down), SPR analysis of MyD88 and RhBG7, RhBGMut, and GST alone (n = 2). (*G*) Colocalization of eGFP-tagged RhBG with mCherry-tagged MyD88. Upper and lower brightness values as set by ImageJ for each channel and are as follows. Red: 31, 255. Green: 0,146. Blue: 0,255. These brightness values are uniform across images. White scale bar represents 1,000 μm. Boxed image refers to zoomed in representative region. (*H*) Colocalization by Pearson's correlation. C2C12 cells were cotransfected with 1 μg of each plasmid. Cells were observed by confocal microscopy with and without ammonia. eGFP images with excitation at 488 nm and emission at 500 to 550 nm, mCherry images with excitation at 568 nm and emission at 580 to 700 nm and WGA for positive marker of membrane images with excitation at ~650 nm and emission at ~668 nm). All coimmunoprecipitation experiments done in n = 1 and live cell and confocal experiments were done in n = 3 biological replicates. ANOVA with Fisher uncorrected LSD post hoc analysis was used for multiple group comparisons.

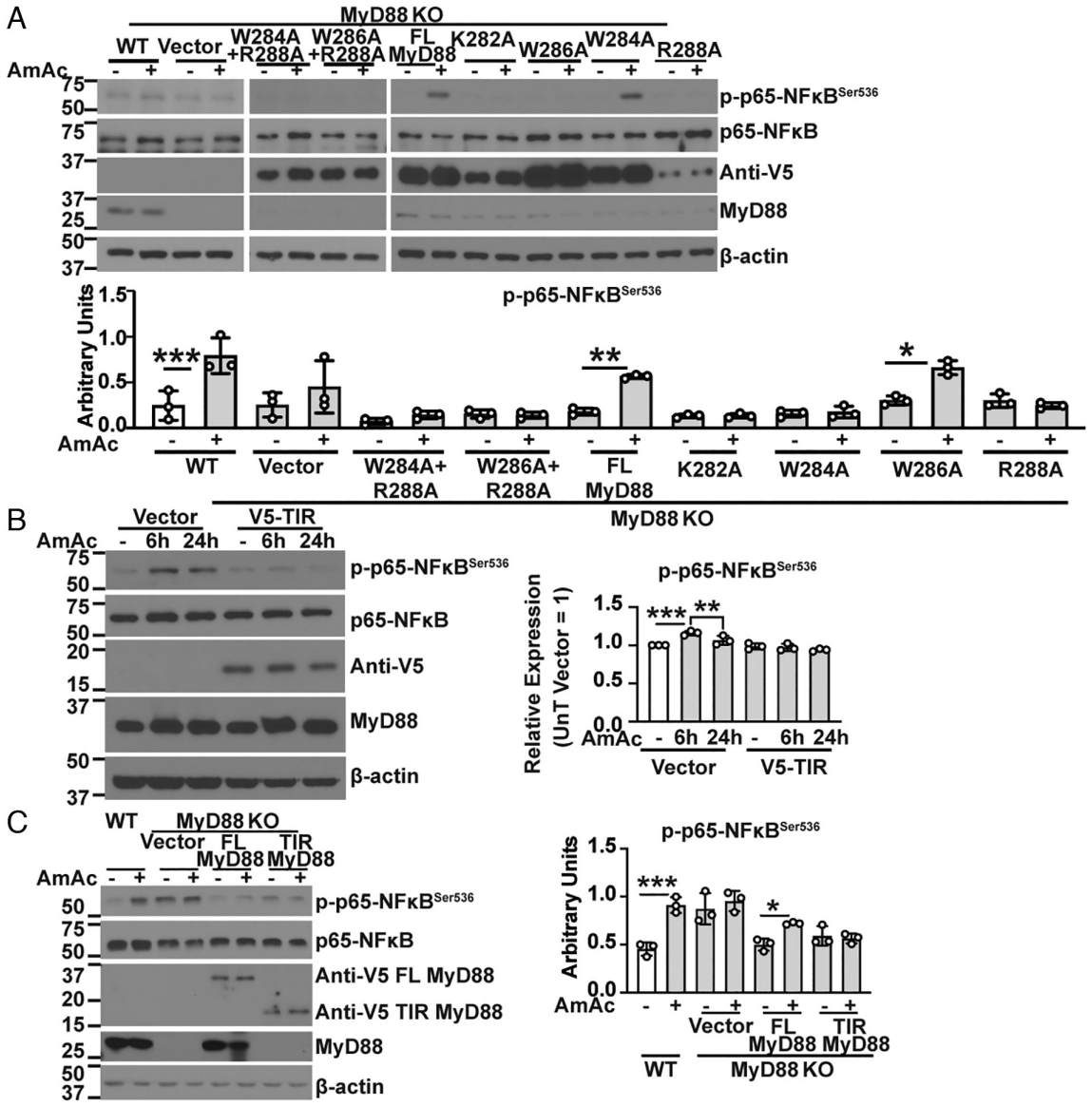

Fig. 5. Deletion of MyD88 reverses ammonia-induced protein synthesis and NFkB activation. Representative immunoblots and densitometries from differentiated murine myotubes treated without/with 10 mM ammonium acetate (AmAc) for the specified times. Representative immunoblots and densitometry of phosphorylated p65-NFκB (*A–C*) in (*A*). WT myotubes and MyD88 knockout (KO) myotubes overexpressing full-length (FL)-MyD88 and MyD88 constructs with mutations of amino acids on the death-domain (interacts with RhBG on docking studies). Empty vector, those with double mutation (W284A+R288A and W286A+R288A), or single mutation on Toll/Interleukin-1 receptor domain of MyD88 (K282A, W284A, W286A, and R288A) were used in transfection studies. (*B*) Overexpression of empty vector or vector with MyD88–TIR domain in WT myotubes. (*C*) WT MyD88 KO myotubes expressing empty vector, full-length MyD88 (FL-MyD88), or TIR-domain of MyD88 (TIR-MyD88). All data mean ± SD from three biological replicates for in vitro. ANOVA with Fisher uncorrected LSD post hoc analysis was used for multiple group comparisons. For panels containing multiple immunoblots, representative blots shown are from the same biological replicate. Representative loading control (β-actin) for panels *A–C* are derived from p-p65-NFκB/p65-NFκB.

unable to bind with RhBG, preventing the activation of p-p65-NFκB (Fig. 5*B*). Knockout of MyD88 and replenishment with the full-length MyD88-FL restore the NFκB activation response to hyperammonemia. However, when only the TIR domain is complemented, NFκB is not activated during hyperammonemia, suggesting that the full-length MyD88 is required for this process (Fig. 5*C*). Expression of constructs with mutation at each of the potential interaction sites showed that only Trp286Ala mutation failed to alter ammonia-induced activation of NFκB, while mutation of the other amino acid residues resulted in loss of ammonia-induced responses, suggesting that these residues (other than Trp286 of MyD88) are important for RhBG binding and downstream signaling. Our data show that several sites on the TIR domain potentially interact with RhBG and are required for mediating downstream signaling responses with activation of NFκB (Fig. 5*A*). Thus, the binding of RhBG to specific locations on MyD88 mediates ammonia-induced, TLR4-independent signaling responses.

We then determined whether the RhBG–MyD88 axis mediates downstream signaling and functional responses during hyperammonemia.

Signaling and Functional Responses During Hyperammonemia Are Mediated by RhBG–MyD88 Axis. We showed that ammonia transport and downstream signaling responses are dependent on RhBG in murine myotubes and in mice with muscle-specific knockout of RhBG (RhBG^{msd}). Hyperammonemia-mediated increase in phosphorylation of p65-NFκB and myostatin expression, lower mTORC1 signaling, and protein synthesis were blocked by RhBG knockout in murine myotubes and gastrocnemius from mice with RhBG^{msd} (Fig. 6 *A–D*). Muscle responses were similar in male and female mice with RhBG^{msd} (*SI Appendix*, Fig. S4 *A*

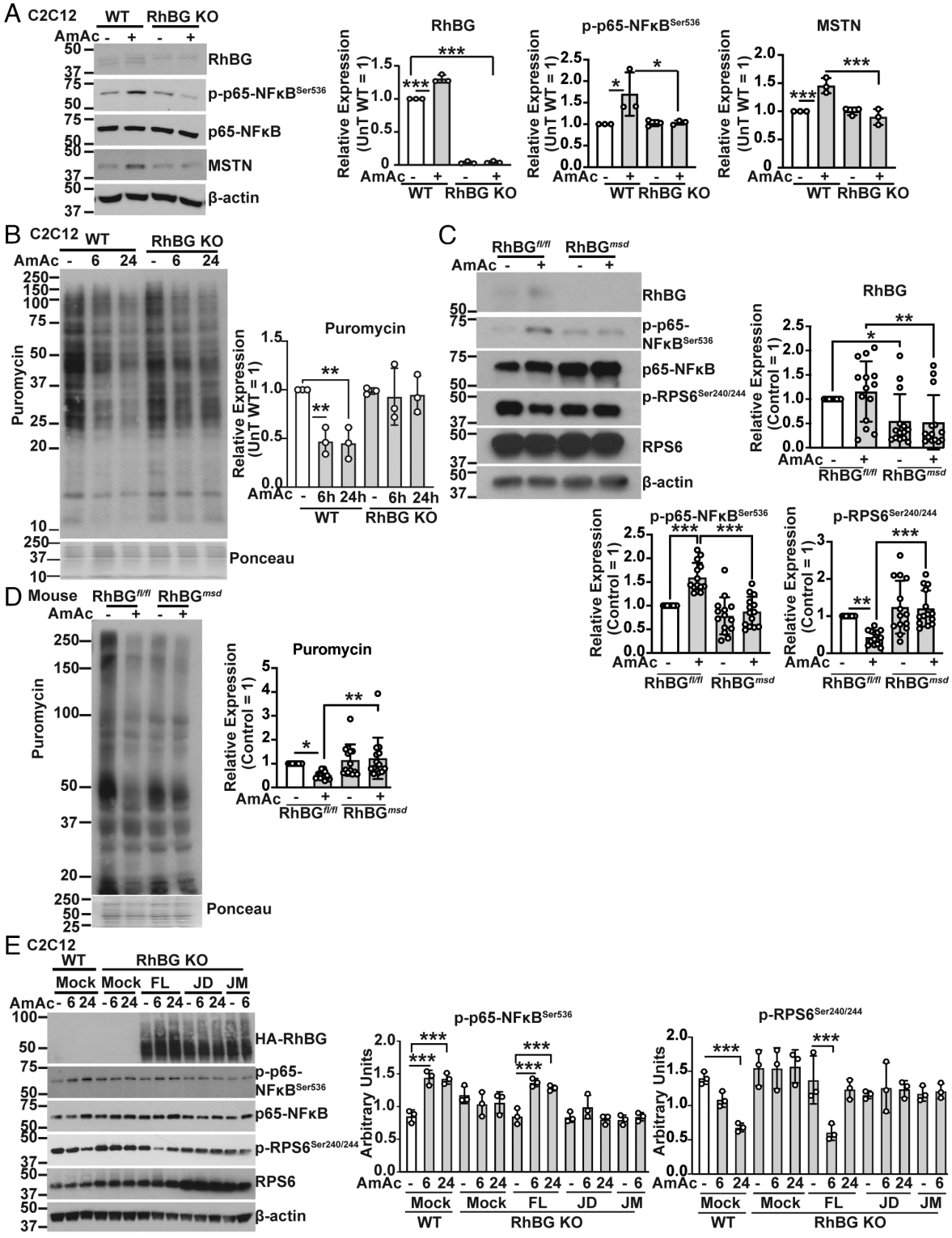

Fig. 6. Hyperammonemia activated NFκB by an RhBG-dependent mechanism. Representative immunoblots and densitometries from differentiated murine myotubes or gastrocnemius muscle from mice with/without hyperammonemia. (*A*) Phosphorylation of p65-NFκB and myostatin expression in myotubes without/with RhBG knockout (KO). (*B*) Representative immunoblots and densitometry (for the indicated conditions) for puromycin incorporation in WT and RhBG KO C2C12 myotubes. (*C*) Representative immunoblots and densitometry of protein synthesis signaling (phosphorylated RPS6 kinase), phosphorylated p65-NFκB in gastrocnemius muscle of floxed (RhBG$^{fl/fl}$), and muscle-specific deletion (RhBG^{msd}) of RhBG (n = 14). (*D*) Representative immunoblots and densitometry of muscle protein synthesis quantified by ex vivo puromycin incorporation in gastrocnemius muscle of RhBG$^{fl/fl}$ and RhBG^{msd} (n = 14). (*E*) Overexpression of HA-tagged RhBG full-length, RhBG J-domain deletion (JD) and FLD mutation in J-domain (JM) in RhBG KO cells restored hyperammonemia induced p65NFκB activation, increased myostatin expression in myotubes. All data mean ± SD from at least three biological replicates for in vitro studies. In vivo studies were done in 12 to 14 wk old male and female C57BL/6 J mice with RhBG^{msd} and parental controls (RhBG$^{fl/fl}$) with 2.5 mM/kg/d ammonium acetate for 28 d or vehicle (phosphate-buffered saline, PBS) delivered by a miniosmotic pump. In vivo data shown in n = 7 mice of each sex per group. *P < 0.05, **P < 0.01, ***P < 0.001. ANOVA with Fisher uncorrected LSD post hoc analysis was used for multiple group comparisons. For panels containing multiple immunoblots, representative blots shown are from the same biological replicate. Representative loading controls (β-actin) originate from the following blots: Panel *A*. RhBG, Panel *C*. p-RPS6/RPS6, Panel *E*. RPS6. Ponceau-S staining was used as loading control for puromycin incorporation.

and *B*). These studies were complemented by restoration of NFκB activation and downstream responses by overexpression of full length, but not domain 7/J-domain-deleted or mutated RhBG constructs (Fig. 6*E*), showing that the cytosolic C-terminal domain of RhBG is critical for signaling responses. Deletion of RhBG also lowered ammonia uptake in myotubes and muscle tissue (in both male and female mice) as measured by ammonia concentrations showing the dual function of this transporter (*SI Appendix*, Fig. S4 *C* and *D*).

We then showed that MyD88 is critical for signaling responses, but not ammonia transport, during hyperammonemia in murine myotubes and skeletal muscle from mice with muscle-specific deletion of MyD88. The hyperammonemia-induced increase in phosphorylation of p65-NFκB in WT cells was not noted in myotubes lacking MyD88 (Fig. 7*A*). Interestingly, despite increased phosphorylation of p65-NFκB in myotubes lacking MyD88 and gastrocnemius skeletal muscle from mice (both male and female mice) with muscle-specific deletion of MyD88 (MyD88^{msd}), signaling and functional responses including myostatin expression, mTORC1 signaling, and lower protein synthesis are not altered (Fig. 7 *A* and *B* and *SI Appendix*, Fig. S5 *A* and *B*). Ammonia transport, measured by ammonia concentrations, is not altered in myotubes lacking MyD88 or in muscle tissue from mice with MyD88^{msd} (*SI Appendix*, Fig. S5 *C* and *D*), showing that RhBG-dependent signaling (but not ammonia transport) is MyD88-dependent. The physiological relevance of these observations was established in mice with MyD88^{msd} (Fig. 7 *C* and *D*).

These data show that ammonia transport requires RhBG, but not MyD88, while intracellular signaling and functional consequences require both RhBG and MyD88, as well as their interaction. We then used multiomics approaches to determine regulatory responses mediated by RhBG and MyD88.

Multiomics Analyses Showed RhBG and MyD88-Dependent Responses. Our data show that the RhBG transceptor–MyD88 adapter protein axis regulates activation of NFκB during hyperammonemia. We then identified shared and unique differentially expressed genes (DEGs) that are targets of NFκB in murine myotubes and gastrocnemius muscle from mice without/with hyperammonemia (*SI Appendix*, Fig. S6*A* and Table S1). There are 87 DEGs during hyperammonemia in myotubes, and highly enriched pathways included TNFα signaling and PI3K-Akt signaling, both of which are known to regulate skeletal muscle protein homeostasis (*SI Appendix*, Fig. S6 *B* and *C*). Of the reported skeletal muscle myokines that are believed to mediate the autocrine and endocrine systemic effects, 36 are NFκB target genes. Among the 36 NFκB targets, 12 are responsive to ammonia; furthermore, the protein synthesis regulatory pathway is enriched in these 12 molecules. (*SI Appendix*, Fig. S6*C*). Similar analyses in mouse muscle tissues also showed 31 DEGs that are NFκB targets, of which seven are myokines, with the potential for endocrine functions in organs beyond the skeletal muscle. Pathways that regulate protein homeostasis and cytokine signaling are enriched in these 31 molecules (*SI Appendix*, Fig. S6*D*). These data show the potential local and systemic effects of skeletal muscle NFκB activation by ammonia.

We then determined the DEGs that are regulated by RhBG and/or MyD88 that are either dependent on or independent of hyperammonemia. We used a previously described approach of horizontal integration across RNAseq datasets (44) in untreated and hyperammonemic myotubes and gastrocnemius muscle tissue from male or female mice (muscle specific deletion or floxed) without or with hyperammonemia. Comparisons of the presence and direction of differential expression changes showed NFκB target genes that are dependent or independent of either RhBG, MyD88, and/or ammonia (*SI Appendix*, Tables S2 and S3). We first compared DEGs in RhBG or MyD88 KO myotubes without or with hyperammonemia. Heatmaps showed significant differences in the DEGs in the NFκB signaling components in myotubes with knockout of RhBG or MyD88, compared to those in WT murine myotubes (Fig. 7*E*). We then determined the NFκB target DEGs that are RhBG-dependent but ammonia-independent (regulated by RhBG in the absence of hyperammonemia), those that are dependent on both RhBG and ammonia (regulated by RhBG during hyperammonemia) and finally, those that are responsive to hyperammonemia but are not dependent on RhBG (DEGs that are potentially regulated by the metabolic responses to ammonia transport or other regulatory mechanisms). STRING analyses for interactions between molecules for each of these groups showed known and currently unidentified molecular regulation between these target genes (*SI Appendix*, Fig. S7 *A–C*). Similar analyses were done for MyD88-regulated genes (*SI Appendix*, Fig. 8 *A–C*). More differences in components of NFκB signaling molecules were noted with MyD88 KO than in RhBG KO. Significant differences were noted in NFκB target DEGs in myotubes with MyD88 KO and RhBG KO that were not altered with hyperammonemia. Finally, we integrated the responses to RhBG and MyD88 without or with hyperammonemia to identify DEGs that were simultaneously regulated by RhBG and MyD88 and those that were regulated independently by these 2 genes in the UpSet plots (*SI Appendix*, Fig. S9). A smaller number of NFκB target DEGs were noted in gastrocnemius muscle from mice with sex differences in target gene regulation as noted in the UpSet plots. Concordant responses across myotubes and muscle tissue on STRING analyses (*SI Appendix*, Figs. S10 and S11) identified a number of currently unknown regulatory molecules in the NFκB target gene pathway that lay the foundation for future studies on transceptor functions. Our untargeted data analyses provide unique insights into membrane transporter–cytosolic protein interaction initiated signaling responses that may be independent of the solute transport function.

Discussion

We show noncanonical initiation of cytosolic adapter protein MyD88 binding to ammonia transporter, RhBG, and consequent downstream signaling responses and functional consequences. Phosphorylation and activation of NFκB, increased myostatin expression, and decreased protein synthesis during hyperammonemia were observed in a comprehensive array of models including murine and hiPSC-derived myotubes and myobundles on biomatrices. Our approach of using multiple models including hiPSC-derived myotubes and human myobundles shows the clinical translational relevance of our observations. Hyperammonemia initiates downstream signaling by interaction of the conserved cytosolic C-terminal domain of RhBG with the TIR domain on MyD88, with resultant increased phosphorylation of IRAK4, recruitment of TRAF6, and subsequent activation of NFκB. Activation of NFκB by the endogenous cytotoxin ammonia is dependent on RhBG, a member of the mammalian ammonia transporter family. Chemical blocking of ammonia transport or genetic depletion of RhBG prevents MyD88–IRAK4 binding. Complementary immunoprecipitation, SPR, and imaging methods show that the cytosolic, C-terminal J-domain on RhBG interacts with MyD88 to initiate downstream signaling responses with activation of NFκB and its transcriptional targets during hyperammonemia. Transport function is mediated by RhBG and was independent of MyD88-dependent signaling responses. These data show that regulated ammonia transporter, RhBG, has an

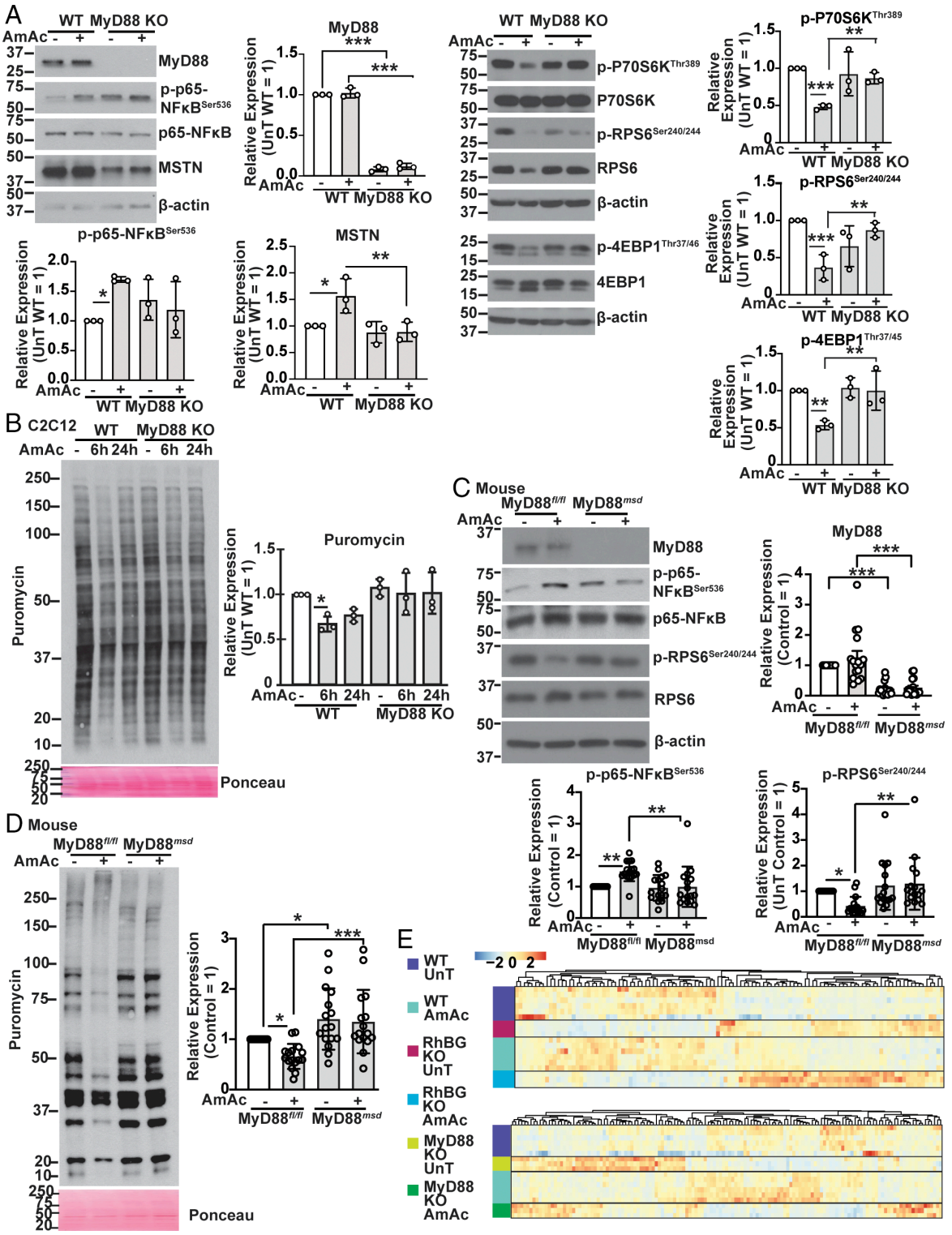

Fig. 7. Hyperammonemia causes RhBG–MyD88 axis–dependent signaling responses. Representative immunoblots and densitometries from differentiated murine myotubes or gastrocnemius muscle from mice with/without hyperammonemia. (*A*) p65-NFκB phosphorylation, myostatin, and mTORC1 signaling expression during hyperammonemia in MyD88 knockout (KO) by CRISPR-Cas9 in myotubes. (*B*) Puromycin incorporation in WT and MyD88 KO C2C12 myotubes that were untreated or treated with 10 mM ammonium acetate (AmAc). (*C*) mTORC1 signaling (phosphorylated-RPS6 kinase) and phosphorylated p65NFκB in gastrocnemius muscle of MyD88 floxed (MyD88$^{fl/fl}$) and muscle specific deletion (MyD88^{msd}) mice (n = 16). (*D*) Muscle protein synthesis quantified by ex vivo puromycin incorporation in gastrocnemius muscle of MyD88$^{fl/fl}$ and MyD88^{msd} (n = 16). Studies done in male and female mice with MyD88^{msd} and parental controls (MyD88$^{fl/fl}$) treated with 28 d AmAc or vehicle (phosphate-buffered saline) delivered by a miniosmotic pump. (*E*) Targeted heat maps of p65NFκB signaling pathway differentially expressed genes (DEG) on transcriptomics from WT (n = 6) and RhBG KO (n = 3) or MyD88 KO (n = 3) myotubes. All data mean ± SD from 3 biological replicates for in vitro. For DEG in myotubes, significance was set at an adjusted-*P* value < 0.05. All data mean ± SD from 3 biological replicates for in vitro data and n = 8 mice of each sex per group for animal studies **P* < 0.05, ***P* < 0.01, ****P* < 0.001. ANOVA with Fisher uncorrected LSD post hoc analysis was used for multiple group comparisons. For panels containing multiple immunoblots, representative blots shown are from the same biological replicate. Representative loading controls (β-actin) originate from the following blots: panel *A*. MSTN, RPS6, 4EBP; panel *C*. MyD88. Ponceau-S staining was used as loading control for puromycin incorporation.

additional signaling function that may be responsible for the metabolic and functional perturbations during hyperammonemia in mammalian tissue/cells.

Skeletal muscle uptake of ammonia occurs during hyperammonemia and results in NFκB-mediated transcriptional upregulation of myostatin, which impairs mTORC1 signaling and decreases protein synthesis (7, 11). Consistent with previous reports, in multiple models of skeletal muscle hyperammonemia including murine and hiPSC myotubes, skeletal muscle from mice, and human patients with cirrhosis (7, 45), we observed phosphorylation and activation of NFκB and increased expression of myostatin. Even though some quantitative differences were noted, the overall effect remained consistent across models. We also show that during hyperammonemia, the classical pathway for phosphorylation and activation of NFκB occurs via sequential signaling from MyD88 to IKKβ. Initiation of MyD88-dependent downstream signaling during hyperammonemia requires the RhBG protein as evidenced by complementary in vitro and in situ interaction studies in cellular systems as well as in skeletal muscle from mice with muscle-specific genetic depletion of RhBG or MyD88.

Interestingly, depletion of MyD88 in myotubes or skeletal muscle results in increased phosphorylation of NFκB but does not affect expression of myostatin, a known transcriptional target of NFκB during hyperammonemia. These data are consistent with data from others that MyD88 deletion inhibits canonical pathways and promotes noncanonical pathways of NFκB activation in myoblasts (46, 47). Our observations in myotubes and skeletal muscle from mice with muscle-specific MyD88 KO suggest that MyD88 potentially inhibits the phosphorylation of NFκB in skeletal muscle in a context-specific manner. Whether such responses occur in other organs/cell types needs to be evaluated in future studies.

Multiomics analyses of RhBG and MyD88 deletion show a number of molecules in the NFκB signaling pathway and target genes are differentially expressed. As expected, MyD88 depletion alters NFκB targets. However, our data showing enrichment of proteins in the B cell receptor, TLR-dependent, and NFκB pathways are unique and lay the foundation for future studies on the mechanisms by which RhBG, a known solute transporter, can alter a number of downstream signaling responses that are dependent and independent of MyD88 and other adapter proteins (Lyn, BLNK).

We provide evidence that RhBG, a regulated ammonia transporter, belongs to a group of increasingly recognized transceptors that have dual transport and signaling functions (32, 36, 48–53). We also show an RhBG-dependent noncanonical activation of the MyD88 signaling pathway that is independent of both TLR4 and ammonia transport function. Targeting the interaction between RhBG and MyD88, specifically interaction sites on these molecules, has the potential to decouple the transport function and adverse signaling and functional consequences during hyperammonemia. The potential to decouple the transport from the signaling function of transceptors shows the biological and translational relevance of our findings.

Our data in mammalian systems show that previously recognized solute transporters can also function by activation of transcription. Unlike the canonical ligand–receptor interaction that initiates transcription, transceptors function during transport of their solutes. Decoupling transport from signaling responses is a potential strategy to regulate solute-dependent cellular dysfunction.

Methods

All animal studies were approved by the Institutional Animal Care Use Committee (0000-1982) at the Cleveland Clinic. All human studies were approved by the Institutional Review Board (CCF IRB 08-546) at the Cleveland Clinic and conformed to the Declaration of Helsinki. A written informed consent was obtained from all subjects prior to the studies.

Details of the methods have been provided in Supplementary methods including strategies for gene editing in murine myoblasts and tissue-specific deletion of RhBG and MyD88.

Data, Materials, and Software Availability. The high-throughput sequencing data (myotube and mouse RNAseq datasets with MyD88 and RhBG KO/msd) first published in the present study have been deposited to the NCBI Sequence Read Archives (SRA) SRA BioProject number PRJNA932336 are are accessible upon publication (54). Previously published mouse skeletal muscle RNAseq data can be accessed with SRA BioProject number PRJNA720399 (GEO: GSE171645) (55) and C2C12 myotubes can be accessed with NCBI SRA BioProject Accession: PRJNA495054 (56).

ACKNOWLEDGMENTS. We express our most sincere appreciation to Gangarao Davuluri for assistance with some of the immunoprecipitation studies and to John Peterson and the Lerner Research Imaging Core for assistance with confocal imaging and analysis. NIH grants: R01 GM119174; R01 DK113196; P50 AA024333; R01 AA021890; 3U01AA026976 - 03S1; U01 AA 026976; R56HL141744;U01 DK061732; 5U01DK062470-17S2; R21 AR 071046. NIH R01-DK45788 and R01-DK107798 (I.D.W.); UH3TR002142 (G.A.T.); K12 HL141952 (A.H.A.) and the American College of Gastroenterology Clinical Research Award and NIH K08 AA 028794 (N.W.). The Fusion Lumos instrument was purchased via an NIH shared instrument grant, 1S10OD023436-01. ERC grant 759107 (F.S.T.). HHS | NIH | National Institute of Diabetes and Digestive and Kidney Diseases, HHS | NIH | National Institute on Alcohol Abuse and Alcoholism.

Author affiliations: [a]Department of Inflammation and Immunity, Lerner Research Institute, Cleveland, OH 44195; [b]Gastroenterology and Hepatology, Lerner Research Institute, Cleveland, OH 44195; [c]Cardiovascular and Metabolic Diseases, Lerner Research Institute, Cleveland, OH 44195; [d]Department of Cell and Developmental Biology, University College London & The Francis Crick Institute, London WC1E6DE, UK; [e]Duke Biomedical Engineering, Duke University, Durham, NC 27708; [f]Pulmonary Medicine, Lerner Research Institute, Cleveland, OH 44195; [g]Cancer Biology, Lerner Research Institute, Cleveland, OH 44195; [h]Division of Nephrology Hypertension, and Renal Transplantation, University of Florida, Gainesville, FL 32610; and [i]Nephrology and Hypertension Section, Gainesville, FL 32610

Author contributions: S.M., N.W., S.S.S., K.D.S., A.K., G.R.S., F.S.T., G.A.T., I.D.W., S.S.K., and S. Dasarathy designed research; S.M., N.W., S.S.S., K.D.S., A.B., A.K., L.N.D., M.D.H., S.K., S. Dastidar, H.P., A.H.A., R.M., G.R.S., F.S.T., G.A.T., S.S.K., and S. Dasarathy performed research; S.M., N.W., S.S.S., K.D.S., A.B., A.K., L.N.D., M.D.H., S.K., S. Dastidar, H.P., V.A., A.H.A., R.M., G.R.S., F.S.T., G.A.T., I.D.W., S.S.K., and S. Dasarathy contributed new reagents/analytic tools; S.M., N.W., S.S.S., K.D.S., A.B., A.K., L.N.D., M.D.H., S.K., S. Dastidar, H.P., A.H.A., R.M., G.R.S., F.S.T., and S. Dasarathy analyzed data; and S.M., N.W., S.S.S., K.D.S., A.B., A.K., S.K., S. Dastidar, V.A., A.H.A., G.R.S., F.S.T., G.A.T., I.D.W., S.S.K., and S. Dasarathy wrote the paper.

1. M. M. Adeva, G. Souto, N. Blanco, C. Donapetry, Ammonium metabolism in humans. *Metabolism* **61**, 1495–1511 (2012).
2. R. E. Shangraw, F. Jahoor, Effect of liver disease and transplantation on urea synthesis in humans: Relationship to acid-base status. *Am. J. Physiol.* **276**, G1145–G1152 (1999).
3. A. H. Lockwood *et al.*, The dynamics of ammonia metabolism in man. Effects of liver disease and hyperammonemia. *J. Clin. Invest.* **63**, 449–460 (1979).
4. S. Dasarathy, M. Hatzoglou, Hyperammonemia and proteostasis in cirrhosis. *Curr. Opin. Clin. Nutr. Metab. Care* **21**, 30–36 (2018).
5. S. Dasarathy *et al.*, Ammonia toxicity: From head to toe? *Metab. Brain Dis.* **32**, 529–538 (2017).
6. O. P. Ganda, N. B. Ruderman, Muscle nitrogen metabolism in chronic hepatic insufficiency. *Metabolism* **25**, 427–435 (1976).
7. J. Qiu *et al.*, Hyperammonemia in cirrhosis induces transcriptional regulation of myostatin by an NF-kappaB-mediated mechanism. *Proc. Natl. Acad. Sci. U.S.A.* **110**, 18162–18167 (2013).
8. M. Merli *et al.*, Muscle depletion increases the risk of overt and minimal hepatic encephalopathy: Results of a prospective study. *Metab. Brain Dis.* **28**, 281–284 (2013).
9. M. Holecek, Evidence of a vicious cycle in glutamine synthesis and breakdown in pathogenesis of hepatic encephalopathy-therapeutic perspectives. *Metab. Brain Dis.* **29**, 9–17 (2014).
10. G. Davuluri *et al.*, Hyperammonaemia-induced skeletal muscle mitochondrial dysfunction results in cataplerosis and oxidative stress. *J. Physiol.* **594**, 7341–7360 (2016).
11. A. Kumar *et al.*, Metabolic reprogramming during hyperammonemia targets mitochondrial function and postmitotic senescence. *JCI Insight* **6** (2021).
12. N. Yalamanchili *et al.*, Distinct cell stress responses induced by ATP restriction in quiescent human fibroblasts. *Front. Genet.* **7**, 171 (2016).
13. M. Kafri, E. Metzl-Raz, G. Jona, N. Barkai, The cost of protein production. *Cell Rep.* **14**, 22–31 (2016).
14. R. L. Smith, M. R. Soeters, R. C. I. Wust, R. H. Houtkooper, Metabolic flexibility as an adaptation to energy resources and requirements in health and disease. *Endocr. Rev.* **39**, 489–517 (2018).

15. S. Dasarathy, Myostatin and beyond in cirrhosis: All roads lead to sarcopenia. *J. Cachexia Sarcopenia Muscle* **8**, 864–869 (2017).
16. A. Oeckinghaus, S. Ghosh, The NF-kappaB family of transcription factors and its regulation. *Cold Spring Harb. Perspect. Biol.* **1**, a000034 (2009).
17. F. Christian, E. L. Smith, R. J. Carmody, The regulation of NF-kappaB subunits by phosphorylation. *Cells* **5** (2016).
18. D. Verzola *et al.*, Toll-like receptor 4 signalling mediates inflammation in skeletal muscle of patients with chronic kidney disease. *J. Cachexia Sarcopenia Muscle* **8**, 131–144 (2017).
19. J. H. Boyd *et al.*, Toll-like receptors differentially regulate CC and CXC chemokines in skeletal muscle via NF-kappaB and calcineurin. *Infect. Immun.* **74**, 6829–6838 (2006).
20. Z. Lin, J. Lu, W. Zhou, Y. Shen, Structural insights into TIR domain specificity of the bridging adaptor Mal in TLR4 signaling. *PLoS One* **7**, e34202 (2012).
21. H. Ohnishi *et al.*, Structural basis for the multiple interactions of the MyD88 TIR domain in TLR4 signaling. *Proc. Natl. Acad. Sci. U.S.A.* **106**, 10260–10265 (2009).
22. A. P. Sinke *et al.*, NFkappaB in the mechanism of ammonia-induced astrocyte swelling in culture. *J. Neurochem.* **106**, 2302–2311 (2008).
23. C. Jefferies *et al.*, Transactivation by the p65 subunit of NF-kappaB in response to interleukin-1 (IL-1) involves MyD88, IL-1 receptor-associated kinase 1, TRAF-6, and Rac1. *Mol. Cell Biol.* **21**, 4544–4552 (2001).
24. H. Wesche, W. J. Henzel, W. Shillinglaw, S. Li, Z. Cao, MyD88: An adapter that recruits IRAK to the IL-1 receptor complex. *Immunity* **7**, 837–847 (1997).
25. T. W. Kim *et al.*, A critical role for IRAK4 kinase activity in Toll-like receptor-mediated innate immunity. *J. Exp. Med.* **204**, 1025–1036 (2007).
26. W. Cui *et al.*, TLR4 ligands lipopolysaccharide and monophosphoryl lipid a differentially regulate effector and memory CD8+ T Cell differentiation. *J. Immunol.* **192**, 4221–4232 (2014).
27. J. C. Rutherford, G. Chua, T. Hughes, M. E. Cardenas, J. Heitman, A Mep2-dependent transcriptional profile links permease function to gene expression during pseudohyphal growth in Saccharomyces cerevisiae. *Mol. Biol. Cell* **19**, 3028–3039 (2008).
28. I. D. Weiner, J. W. Verlander, Molecular physiology of the Rh ammonia transport proteins. *Curr. Opin. Nephrol. Hypertens* **19**, 471–477 (2010).
29. A. Rogato, E. D'Apuzzo, M. Chiurazzi, The multiple plant response to high ammonium conditions: The Lotus japonicus AMT1; 3 protein acts as a putative transceptor. *Plant Signal Behav.* **5**, 1594–1596 (2010).
30. T. Caner *et al.*, Mechanisms of ammonia and ammonium transport by rhesus-associated glycoproteins. *Am. J. Physiol. Cell Physiol.* **309**, C747–758 (2015).
31. S. Kant *et al.*, Ethanol sensitizes skeletal muscle to ammonia-induced molecular perturbations. *J. Biol. Chem.* **294**, 7231–7244 (2019).
32. J. M. Thevelein, K. Voordeckers, Functioning and evolutionary significance of nutrient transceptors. *Mol. Biol. Evol.* **26**, 2407–2414 (2009).
33. H. S. Hundal, P. M. Taylor, Amino acid transceptors: Gate keepers of nutrient exchange and regulators of nutrient signaling. *Am. J. Physiol. Endocrinol. Metab.* **296**, E603–613 (2009).
34. J. M. Thevelein *et al.*, Novel mechanisms in nutrient activation of the yeast protein kinase A pathway. *Acta Microbiol. Immunol. Hung.* **55**, 75–89 (2008).
35. J. Kriel, S. Haesendonckx, M. Rubio-Texeira, G. Van Zeebroeck, J. M. Thevelein, From transporter to transceptor: Signaling from transporters provokes re-evaluation of complex trafficking and regulatory controls: Endocytic internalization and intracellular trafficking of nutrient transceptors may, at least in part, be governed by their signaling function. *Bioessays* **33**, 870–879 (2011).
36. G. Diallinas, Transceptors as a functional link of transporters and receptors. *Microb. Cell* **4**, 69–73 (2017).
37. H. N. Kankipati, M. Rubio-Texeira, D. Castermans, G. Diallinas, J. M. Thevelein, Sul1 and Sul2 sulfate transceptors signal to protein kinase A upon exit of sulfur starvation. *J. Biol. Chem.* **290**, 10430–10446 (2015).
38. M. C. Lorenz, J. Heitman, The MEP2 ammonium permease regulates pseudohyphal differentiation in Saccharomyces cerevisiae. *EMBO J.* **17**, 1236–1247 (1998).
39. F. Gruswitz *et al.*, Function of human Rh based on structure of RhCG at 2.1 A. *Proc. Natl. Acad. Sci. U.S.A.* **107**, 9638–9643 (2010).
40. S. Dasarathy *et al.*, Sarcopenia associated with portosystemic shunting is reversed by follistatin. *J. Hepatol.* **54**, 915–921 (2011).
41. J. Ninomiya-Tsuji *et al.*, The kinase TAK1 can activate the NIK-I kappaB as well as the MAP kinase cascade in the IL-1 signalling pathway. *Nature* **398**, 252–256 (1999).
42. C. Lopez *et al.*, The ammonium transporter RhBG: Requirement of a tyrosine-based signal and ankyrin-G for basolateral targeting and membrane anchorage in polarized kidney epithelial cells. *J. Biol. Chem.* **280**, 8221–8228 (2005).
43. N. Zidi-Yahiaoui *et al.*, Human Rhesus B and Rhesus C glycoproteins: Properties of facilitated ammonium transport in recombinant kidney cells. *Biochem. J.* **391**, 33–40 (2005).
44. N. Welch *et al.*, Integrated multiomics analysis identifies molecular landscape perturbations during hyperammonemia in skeletal muscle and myotubes. *J. Biol. Chem.* **297**, 101023 (2021).
45. G. Davuluri *et al.*, Impaired ribosomal biogenesis by noncanonical degradation of beta-catenin during hyperammonemia. *Mol. Cell Biol.* **39** (2019).
46. S. M. Hindi *et al.*, MyD88 promotes myoblast fusion in a cell-autonomous manner. *Nat. Commun.* **8**, 1624 (2017).
47. A. Parveen *et al.*, MyD88-mediated signaling intercedes in neurogenic muscle atrophy through multiple mechanisms. *FASEB J.* **35**, e21821 (2021).
48. Y. Wang *et al.*, Fungal commensalism modulated by a dual-action phosphate transceptor. *Cell Rep.* **38**, 110293 (2022).
49. X. Wang *et al.*, A transceptor-channel complex couples nitrate sensing to calcium signaling in Arabidopsis. *Mol. Plant* **14**, 774–786 (2021).
50. M. Scalise *et al.*, Insights into the transport side of the human SLC38A9 transceptor. *Biochim. Biophys. Acta Biomembr.* **1861**, 1558–1567 (2019).
51. V. Cointry, G. Vert, The bifunctional transporter-receptor IRT1 at the heart of metal sensing and signalling. *New Phytol.* **223**, 1173–1178 (2019).
52. B. van den Berg, S. Lister, J. C. Rutherford, Ammonium transceptors: Novel regulators of fungal development. *PLoS Pathog.* **15**, e1008059 (2019).
53. G. Tena, Metal transceptor. *Nat. Plants* **4**, 191 (2018).
54. N. Welch, S. Dasarathy, Muscle-specific gene deletion in mice. NCBI BioProject. https://www.ncbi.nlm.nih.gov/bioproject/PRJNA932336. Deposited 7 February 2024.
55. N. Welch, S. Dasarathy, Integrated molecular landscape perturbations underlie cellular responses during hyperammonemia. NCBI Gene Expression Omnibus. https://www.ncbi.nlm.nih.gov/geo/query/acc.cgi?acc=GSE171645. Deposited 27 July 2021.
56. G. Davuluri, N. Welch, S. Dasarathy, Ammonia treated C2C12 myotubes RNA sequencing. NCBI BioProject. https://www.ncbi.nlm.nih.gov/bioproject/PRJNA495054. Deposited 8 October 2018.